ARMY RESEARCH LABORATORY

Diffractive Design: Two Examples from an Optical Analog-to-Digital Converter

by Joseph N. Mait

ARL-MR-336

February 1997

The findings in this report are not to be construed as an official Department of the Army position unless so designated by other authorized documents.

Citation of manufacturer's or trade names does not constitute an official endorsement or approval of the use thereof.

Destroy this report when it is no longer needed. Do not return it to the originator.

Army Research Laboratory
Adelphi, MD 20783-1197

ARL-MR-336 **February 1997**

Diffractive Design: Two Examples from an Optical Analog-to-Digital Converter

Joseph N. Mait
Sensors and Electron Devices Directorate

Abstract

In this report, I present the designs of two diffractive optical array generators used in an optical analog-to-digital converter. The designs follow a procedure that I developed for the design of general diffractive optical elements. I consider both separable and nonseparable approaches to designing a 5×5 binary-phase fanout, and discuss indirect and direct optimizations for the nonseparable approach. I use a nonseparable approach with direct optimization to design an 8-phase-level 7×7 array generator.

Contents

Figures

Tables

1. Introduction

Diffractive optical elements (DOEs) are thin optical elements with functions that derive from diffraction, as opposed to reflection or refraction. Diffractive optics both supplement and complement refractive optics. That is, although a DOE can be used to replace refractive components, it can also be used in combination with refractive optics to enhance the overall performance of an optical system. Most important is that DOEs can be designed and fabricated to implement functions that refractive and reflective components cannot implement.

The widespread application of DOEs requires an understanding of diffractive design. Although archived publications on this topic are available [1,2], they typically concentrate on theory and provide few examples. The objective of this report is to highlight, through example, the important issues in diffractive design. The two DOEs I discuss here were produced for an optical analog-to-digital (A/D) converter designed by MAJ Barry Shoop of the U.S. Military Academy [3].

Section 2 includes a brief review of diffractive design, and sections 3 and 4 show design examples.

2. Diffractive Design

The design of a DOE incorporates three primary steps: (1) understanding the physics of the design problem (analysis), (2) translating that physical understanding into mathematics and defining an appropriate optimization problem (synthesis), and (3) executing the design and fabricating the element (implementation). Following is a further breakdown of each step.

2.1 Analysis

Step 1: Understand the physics of image formation using the DOE.

Step 2: Understand the fabrication of the DOE from data generated by computer.

By "understand" I mean to imply the selection of a model. The coherent Fourier transformer shown in figure 1 is a valid representation of the optics for the two examples that I consider here. Under the assumptions of scalar diffraction theory, the DOE is a physically thin element that modulates the complex wave amplitude of an incident wavefield according to

$$P(u,v) = A(u,v)\exp\left[j\theta\,(u,v)\right]. \tag{1}$$

If the source illumination is a spatially coherent, quasi-monochromatic plane wave with wavelength λ, a Fourier transform relationship exists between the diffractive element $P(u,v)$ in the pupil plane and its response $p(x,y)$ in the image plane [4],

$$p(x,y) = \int\int P(u,v)\exp\left[j\frac{2\pi}{\lambda f}\,(ux+vy)\right]dudv\,.^{*} \tag{2}$$

where f is the focal length of the lens.

Assuming that a multistep etch procedure is used to fabricate the DOEs [5], if the fabrication process from computer-generated data to diffractive element is linear and introduces no errors, I can model the DOE as a multilevel quantized phase element (i.e., $A(u,v) = 1$ and $\theta(u,v) = 2\pi\ell/L$, $\ell = [0; L-1]$).

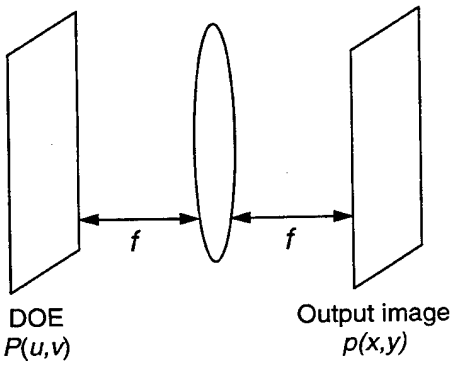

Figure 1. Coherent optical Fourier transformer.

*I have ignored complex scale factors.

The DOEs that I considered each produce an array of point sources when illuminated by a single point source and are, therefore, referred to as array generators. I represent the desired array by $q(x,y)$,

$$q(x,y) = \sum_{n=1}^{N} q_n \delta\left(x - x_n, y - y_n\right), \tag{3}$$

where N is the total number of spots in the array, (x_n, y_n) are their spot locations, and the phasor q_n is their spot magnitude and phase. If the spot locations (x_n, y_n) are rational, the Fourier transform $Q(u,v)$ of $q(x,y)$ is periodic and, therefore, $P(u,v)$ must also be periodic,

$$P(u,v) = \tilde{P}(u,v) \ ** \ \mathrm{repl}(u,v), \tag{4a}$$

where $\tilde{P}(u,v)$ is a single period representation of the array generator, with unity extent along both axes. The two-dimensional convolution (represented by * *) of $\tilde{P}(u,v)$ with the replicating function $\mathrm{repl}(u,v)$ tiles the Fourier plane (see fig. 2). As a consequence, the points in image space at which the generated array has value are determined by the lattice array $\mathrm{samp}(x,y)$,

$$p(x,y) = \tilde{p}(x,y) \ \mathrm{samp}(x,y). \tag{4b}$$

The functions $\mathrm{repl}(u,v)$ and $\mathrm{samp}(x,y)$ form a Fourier transform pair.

2.2 Synthesis

Step 3: Define the design metric.

Step 4: Define the optimization problem.

The fidelity of an array generator is based on its ability to generate the desired spot array with high diffraction efficiency and minimum intensity error. Diffraction efficiency is the ratio of the energy diffracted into the desired signal to the total energy in the image plane,

$$\eta = \frac{\int\int\limits_{(x,y)\in X} |p(x,y)|^2 dxdy}{\int\limits_{-\infty}^{\infty}\int\limits_{-\infty}^{\infty} |p(x,y)|^2 dxdy} = \frac{\int\int\limits_{(x,y)\in X} |p(x,y)|^2 dxdy}{\int\limits_{-\infty}^{\infty}\int\limits_{-\infty}^{\infty} |P(u,v)|^2 dudv} =$$

$$\int\int\limits_{(x,y)\in X} |p(x,y)|^2 dxdy = \sum_{n=1}^{N} |p_n|^2. \tag{5}$$

Intensity error is

$$e_{int} = \int\int\limits_{(x,y)\in X} \left| |p(x,y)|^2 - \alpha \, |q(x,y)|^2 \right|^2 dxdy =$$

$$\sum_{n=1}^{N} \left| |p_n|^2 - \alpha \, |q_n|^2 \right|^2. \tag{6}$$

My use of the scale factor α indicates that the absolute intensity of the response is not critical; rather, the response $p(x,y)$ should exhibit the shape described by $q(x,y)$. This is defined as an application of scale freedom [6]. However, a scale factor $\alpha_{\min}$ exists that minimizes e_{int}:

$$\alpha_{\min} = \frac{\int\int_{(x,y)\in X} |p(x,y)|^2 \, |q(x,y)|^2 \, dxdy}{\int\int_{(x,y)\in X} |q(x,y)|^4 \, dxdy} = \frac{\sum_{n=1}^{N} |p_n|^2 |q_n|^2}{\sum_{n=1}^{N} |q_n|^4}. \quad (7)$$

The scale $\alpha_{\min}$ yields the minimum fluctuation from the desired intensity by the generated intensity, which is represented in figure 3.

The physical extent of the detector in the image plane and the fact that it responds to intensity influence the definition of the error. I am concerned only with the intensity of the response within the signal window x; the phase within the signal window and the total response outside of the signal window are unimportant. Thus, I am also using phase-freedom and complex-wave amplitude in my designs [6]. However, a tradeoff exists

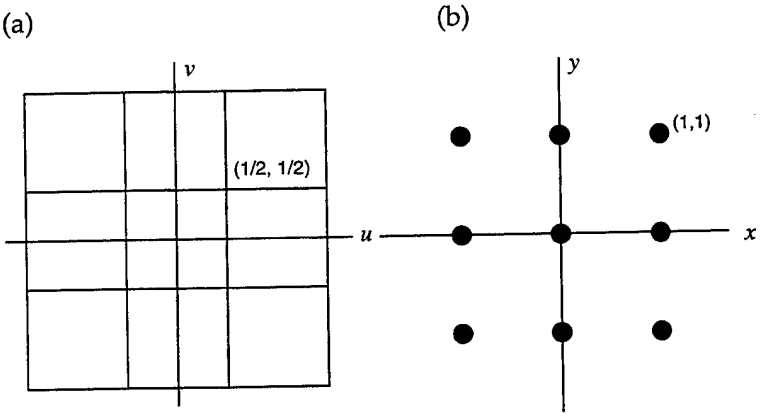

Figure 2. Transform relationship between Fourier replicating function and lattice of image sampling points that it generates: (a) tiling of Fourier plane with $P(u,v)$ by $\text{repl}(u,v)$; (b) lattice image sample points $\text{samp}(x,y)$ by $\text{repl}(u,v)$.

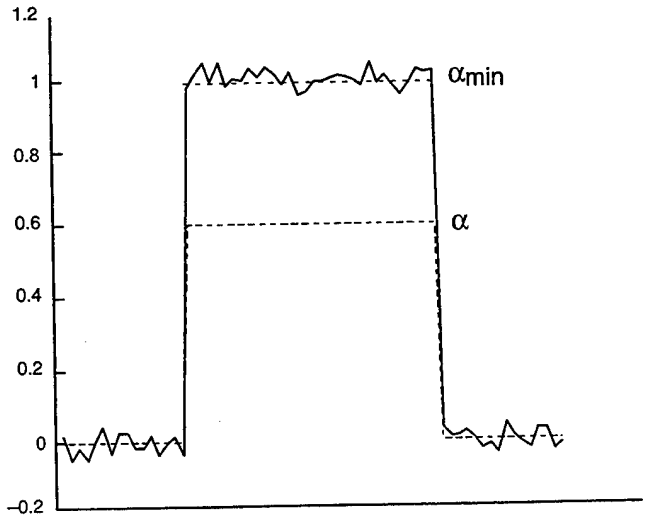

Figure 3. Significance of scale factor $\alpha_{\min}$ in determining intensity error.

between diffraction efficiency and error (i.e., minimum error can be achieved by reducing diffraction efficiency). Likewise, high diffraction efficiency can be achieved by allowing for large levels of error. One determines these measures *after* the design is complete.

For optimal design, it is necessary to define a metric that accounts for this tradeoff *before* beginning the work, and to use it within an optimization routine. I have used

$$e_{ub} = \sum_{n=1}^{N} \left| |p_n|^2 - \alpha_{ub} |q_n|^2 \right|^2 , \tag{8}$$

where $\alpha_{ub} = \eta_{ub}/N$ and η_{ub} is the diffraction efficiency upper bound [7],

$$\eta_{ub} = \frac{\left[\int_{-1/2}^{1/2} \int_{-1/2}^{1/2} |Q(u,v)| \, du dv \right]^2}{\int_{-1/2}^{1/2} \int_{-1/2}^{1/2} |Q(u,v)|^2 \, du dv}. \tag{9}$$

Thus, the intensity distribution $\alpha_{ub}|q(x,y)|^2$ represents the maximum array intensity that a phase-only DOE can generate. Although η = 100 percent also represents an upper bound on diffraction efficiency, it is too general to be effective; η_{ub} provides more specific information about the particular design of interest. Because $\alpha_{ub}|q(x,y)|^2$ represents a fixed, upper limit in the space of solutions, the metric e_{ub} is an absolute distance measurement.

2.3 Implementation

Step 5: Select a design algorithm and performing the optimization.

Step 6: Fabricate the DOE from the computer-generated data.

Step 7: Test the DOE.

Steps 5 to 7 are straightforward—select the design, fabricate the DOE, and test its performance in the system—but require many practical decisions and, most importantly, a considerable expenditure of resources.

One of these decisions is determining the physical dimensions and minimum features of the DOE before fabrication. The transform relationship between $P(u,v)$ and $p(x,y)$ assumes that $\tilde{P}(u,v)$ has unit extent along both axes. The spots of $p(x,y)$, therefore, are located at integer multiples of λf. For an arbitrary spot spacing d along one axis, the unit period width W is

$$W = \lambda f / d. \tag{10}$$

If the total length of the DOE is D in one dimension, the number of replicas M of the unit period is

$$M = D/W. \tag{11}$$

Further, if the minimum feature is Δ, the number of addressable features L within the unit period is

$$L = W/\Delta. \tag{12}$$

The total number of addressable features in the element is its space-bandwidth product (SBWP) S,

$$S = ML = D/\Delta. \tag{13}$$

For example, for a 1-cm, one-dimensional element written with 1-μm features, $S = 10^4$. Due to the fact that, at a minimum, it takes two features to code a single value in the desired response, the SBWP has a direct impact on design. Therefore, the maximum number of points that can be specified in $q(x, y)$ is $S/2$.

3. Design Examples

3.1 Example 1: (0, π)-Binary-Phase 5×5 Fanout

The first design example is a (0, π)-binary-phase 5×5 fanout (a "fanout" implies that all spots have equal intensity). The illumination wavelength λ = 850 nm and the focal length of the lens f = 50 mm. The spacing between spots along both axes is d = 250 μm. The grating period is, therefore, 170×170 μm^2. The element size $D_x \times D_y = 5 \times 5$ mm^2, which implies that the unit cell is repeated 30×30 times.

For this example, two approaches to design are possible: separable and nonseparable. A two-dimensional function is separable if its behavior along one axis is independent of its position on the other axis. In a separable design, one considers the desired performance along the horizontal and vertical axes separately, and crosses the one-dimensional results to construct a two-dimensional array generator. A nonseparable design considers the two-dimensional performance as a whole.

The design requires determination of the upper bound on the diffraction efficiency. Except for the constraints imposed on array phase by a binary-phase array generator, which I discuss below, determination of the diffraction efficiency upper bound is independent of any fabrication considerations. The upper bound represents the theoretical upper limit on the diffraction efficiency with which the desired array can be generated.

The expression for the diffraction efficiency upper bound requires complete specification of the desired array $q(x, y)$ in terms of magnitude and phase. The design, however, considers only the intensity $|q(x, y)|^2$, and so only the magnitude $|q(x, y)|$ is specified. This limitation is, however, to one's advantage in terms of high diffraction efficiency design, since the freedom to specify phase allows a choice of the phase that generates the highest diffraction efficiency.

To determine this phase, the expression for the diffraction efficiency upper bound with respect to the array phase [7,8] must be maximized. However, a binary-phase DOE generates a response that is Hermitian (i.e., $p(x, y) = p^*(-x, -y)$); therefore, the phase of $q(x, y)$ is not completely arbitrary, but must be odd. The array phase $\theta_{ub}(x, y)$,

$\theta_{ub}(x, y)$	$x = -2$	$x = -1$	$x = 0$	$x = 1$	$x = 2$
$y = -2$	−1.3915	1.2433	−1.2749	1.6429	0.7962
$y = -1$	−0.1648	1.6689	2.3327	−0.0511	−0.3013
$y = 0$	1.5014	−2.5544	−3.1416	2.5544	−1.5014
$y = 1$	0.3013	0.0511	−2.3327	−1.6689	0.1648
$y = 2$	−0.7962	−1.6429	1.2749	−1.2433	1.3915

yields an upper bound of 78.88 percent; thus, $\alpha_{ub} = 31.5 \times 10^{-3}$. The real-valued Fourier transform $Q_{ub}(u, v)$ of $q_{ub}(x, y) = |q(x, y)| \exp[j\theta_{ub}(x, y)]$ is represented in figure 4.

3.1.1 *Separable Design*

The nature of the 5×5 fanout allows construction of a two-dimensional array generator from a single one-dimensional, 5-spot fanout. Further, the array generator's binary-phase and small number of spots allow use of so-called Dammann design techniques [2,9].

To achieve a uniform-intensity spot array, Dammann recognized that a one-dimensional, $(0, \pi)$-binary-phase array generator can be represented completely by the locations z_k at which its phase transitions occur. Consider figure 5 and the representation of $\tilde{P}(u)$ in terms of a binary amplitude function $\Sigma(u)$,

$$\tilde{P}(u) = 2\Sigma(u) - \text{rect}(u), \tag{14a}$$

where

$$\Sigma(u) = \sum_{\substack{k=1 \\ k \text{ odd}}}^{K-1} \text{rect}\left[\frac{u - (z_{k+1} + z_k)/2}{z_{k+1} - z_k}\right]. \tag{14b}$$

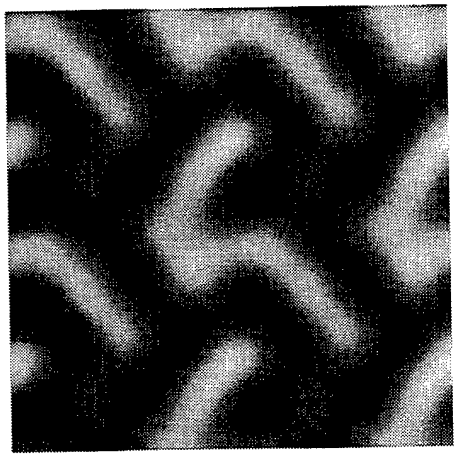

Figure 4. Representation of $Q_{ub}(u, v)$ for a 5×5 fanout (two periods are shown).

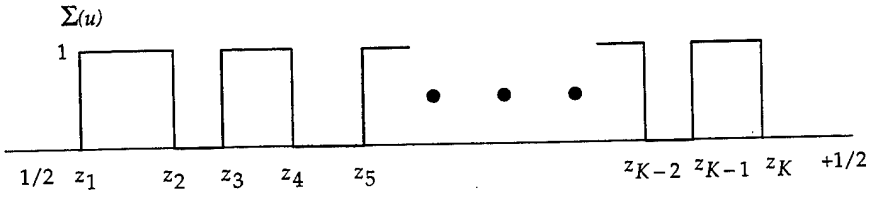

Figure 5. Binary amplitude distribution $\Sigma(u)$ used to describe a one-dimensional binary-phase array generator.

If $\mathrm{repl}(u) = \mathrm{comb}(u)$, where $\mathrm{comb}(u) = \sum_{n=-\infty}^{\infty} \delta(u-n)$, then, by virtue of the self-transforming properties of the comb-function, the generated array is

$$p(x) = \sum_{n=-\infty}^{\infty} [2\sigma(n) - \mathrm{sinc}(n)]\, \delta(x-n)\,, \tag{15a}$$

where

$$\sigma(n) = \sum_{\substack{k=1 \\ k \text{ odd}}}^{K-1} (z_{k+1} - z_k)\, \mathrm{sinc}\left[(z_{k+1} - z_k)\, n\right] \exp\left[j\pi\,(z_{k+1} + z_k)\, n\right]. \tag{15b}$$

The comb-function replication generates a spot array that assumes values at integer locations in the image plane and, from symmetry, generates an array that has an odd number of spots. To generate an even number of spots, it is necessary to use an alternative replication [10],

$$P(u) = \tilde{P}(u) * \exp(j\pi u)\mathrm{comb}(u)\,, \tag{16a}$$

which generates

$$p(x) = \tilde{p}(x)\mathrm{comb}(x - 1/2). \tag{16b}$$

The π-phase change between replicas acts as a spatial carrier to translate all spots off axis without changing the spacing between sample points. In conjunction with the symmetry imposed by the grating, this implies that the array has an even number of spots.

To determine the phase-transition locations, the generated intensity $|p(x)|^2$ must be set proportional to the desired intensity $|q(x)|^2$, $|p(x)|^2 = \alpha|q(x)|^2$, for $x = [0, N]$. Due to the Hermitian symmetry imposed by a (0, π)-binary-phase array generator, the constant α is real-valued. The $N+1$ real-valued equations can be solved for α and the phase transitions z_k, $k = [1, K]$. Because the system of equations is nonlinear, there is no constraint that the number of unknowns must equal the number of equations—the total number of transitions K is arbitrary. However, in general, the fewer the number of phase transitions, the higher the diffraction efficiency.

The phase transitions for many one-dimensional, Dammann gratings ((0, π)-binary phase gratings) can be found in several references (for example, [11,12]). The phase transitions within a unit cell of length unity that generate a 5-spot fanout with high diffraction efficiency are shown in table 1. The value of α for the one-dimensional problem is 0.1548, the square of which (24.0×10^{-3}) is the value for the two-dimensional problem.

Table 1. Phase transitions in a Dammann grating to produce a 5-spot array generator.

Unit cell	End point	z_1	z_2	z_3	z_4	End point
Unit interval	−0.50000	−0.36766	−0.01930	0.01930	0.36766	0.50000
170-μm period (μm)	0.00	22.50	81.72	88.28	147.50	170.00
Quantized 170-μm period (μm)	0.0	22.0	81.4	88.0	147.4	170.5
Quantized unit interval	−0.50000	−0.37097	−0.02258	0.01613	0.36452	0.50000

Fabrication requires the conversion of the normalized locations of phase transition to distances through multiplication by the grating period and addition of an appropriate shift; these values are also indicated in the table. Unfortunately, the fabrication process does not have unlimited resolution, and distances must be quantized according to the minimum placement resolution and minimum features of the fabrication technology. Typical values for fabrication technology available today are 0.1-μm placement resolution and 1-μm minimum feature. Table 1 includes the phase transitions for a minimum feature of 1.1 μm. The impact on fabrication parameters is shown in table 2.

The separable two-dimensional pattern generated from the one-dimensional structure is represented in figure 6. The fidelity of the generator's response is summarized in table 3. The generator's intensity response, as well as that of all the other designs, is listed in appendix A. For a fanout element, in which case $|q_n| = 1$, equation (7) reduces to

$$i_{\text{ave}} = \alpha_{\min} = \frac{1}{N} \sum_{n=1}^{N} |p_n|^2. \tag{17}$$

Further, I define e_{rms} as

$$e_{\text{rms}} = \sqrt{e_{\text{int}}/N}\ . \tag{18}$$

The ratio $e_{\text{rms}}/i_{\text{ave}}$ is, in essence, a per-spot measure of the noise fluctuations (i.e., a noise-to-signal ratio per spot). The tradeoff between diffraction efficiency and error is clearly evident in table 3.

3.1.2 *Nonseparable Design*

In the previous section, separable design of the array generator used analytic techniques to determine the locations of phase transition; however, in general, the desired design metric must be optimized explicitly. This is the approach that I take in this section. The optimization problem can be stated in the following way.

Problem 1: Minimize e_{ub} over $P(u,v) = A(u,v)\ \exp[j\theta(u,v)]$ subject to $A(u,v) = 1$ and $\theta(u,v) = \{2\pi\ell/L; \ell = 1, 2, \ldots, L-1\}$.

Table 2. Summary of fabrication parameters for 5 × 5-spot array generators.*

Design $\lambda = 850$ nm, $f = 50$ mm	Δ_x (μm)	L_x	W_x (μm)	M_x	D_x (mm)	d_x (μm)
Desired	—	—	170.00	—	5.000	250.00
Separable	1.10	155	170.50	30	5.115	249.27
Nonseparable	1.33	128	170.24	30	5.107	249.65

**Due to square nature of array generator, features in only one dimension are indicated.*

Figure 6. Representation of Dammann-designed separable array generator (two replications of the unit cell are shown).

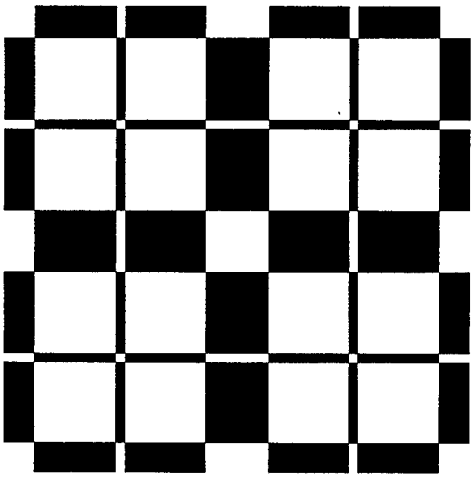

Table 3. Summary of response characteristics for 5 × 5-spot array generators.

Array generator	η (%)	i_{ave} ($\times 10^{-3}$)	e_{rms} ($\times 10^{-3}$)	e_{rms}/i_{ave} (%)	Order (computing time)
Upper bound	78.88	31.5	—	—	Minutes
Dammann grating	59.89	24.0	0.06	0.24	Negligible
Quantized design	80.58	32.2	9.60	29.65	Negligible
Iterated design	69.67	27.9	1.70	5.98	Minutes
Annealed design	76.34	30.5	1.40	4.46	Hours

Two basic approaches to solving problem 1 have emerged in the DOE literature—one that is direct and one that is indirect [2]. In an indirect design, the unconstrained design problem must be solved.

Problem 2: Minimize e_{ub} over $P(u, v)$.

The solution of problem 2 $Q_{ub}(u, v)$ is then mapped onto the fabrication constraints. Mapping can be as simple as quantization, or it can be an optimal routine. In a direct design, the constraints of fabrication must be applied directly, as in problem 1.

Due to fabrication constraints, the ordinate values (u, v) are not continuous, but discrete (i.e., $(u, v) = (i_u\Delta, i_v\Delta)$, where Δ is the minimum feature size and i_u and i_v are integers. To accommodate the use of the fast Fourier transform in the solution of problems 1 and 2, I divided the unit cell into 128 minimum features, which correspond to Δ = 1.33 μm. The fabrication parameters for nonseparable design are summarized in table 2. I solve problems 1 and 2 in the following sections.

3.1.3 *Indirect Design*

Indirect design of the array generator requires the solution of problem 2, which, as I stated, is the complex function $Q_{ub}(u, v)$. The second step in the design is the application of the fabrication constraints, which, for this problem, implies that the DOE can assume only two values: –1 and +1. This constraint can be applied by simple quantization, which yields the array generator represented in figure 7. Its performance, which is notably poor, is summarized in table 3. It should not be concluded from this summary, however, that indirect methods always produce poor results. In this case, the poor results were a consequence of the parameters particular to this design.

3.1.4 *Direct Design*

Two general nonlinear optimization algorithms capable of solving problem 1 are represented in figure 8 [13]. The operator T reflects the understanding (from step 1) of the influence that the DOE has on the image it produces, and the operator E is the design metric.

Fienup [13] refers to the algorithms in figures 8(a) and (b) as error-reduction and input-output; however, to indicate the nature of data flow, I prefer the nomenclature bidirectional and unidirectional. Note that use of a bidirectional algorithm implies not only an understanding of the operator T, but also an understanding of its inverse, T^{-1} (i.e., an understanding of how variations in the response affect the DOE). Under my assumptions, the system T is modeled by a Fourier transform, which is easily inverted. Therefore, figure 8(a) represents the iterative Fourier transform algorithm (IFTA) [6,13,14].

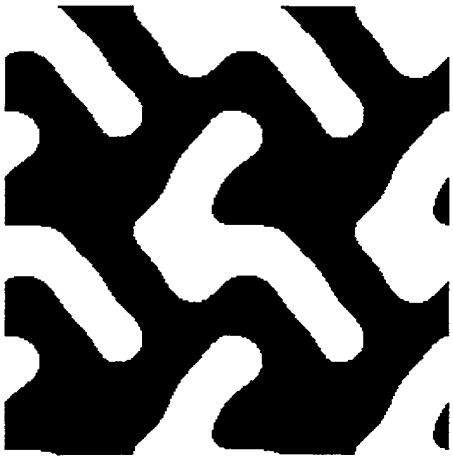

Figure 7. Representation of indirect design of a nonseparable array generator (two replications of the unit cell are shown).

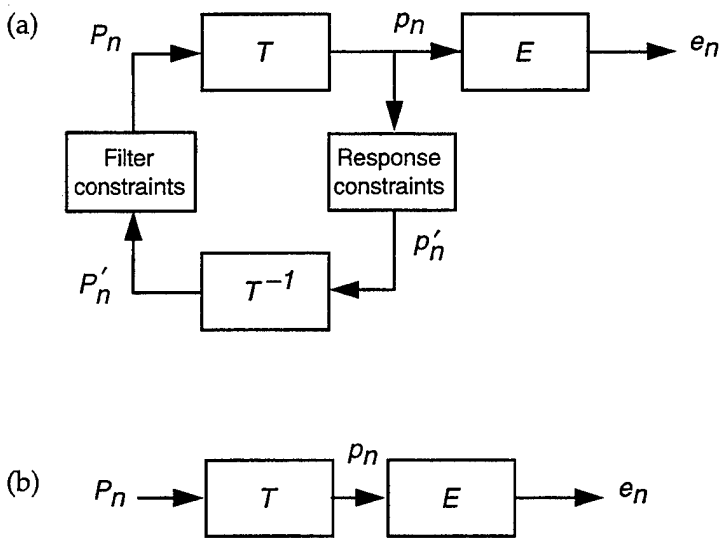

Figure 8. Optimization algorithms used for design: (a) bidirectional; (b) unidirectional.

Although the IFTA is simple in its implementation, it is prone to stagnate in local minima. To overcome this problem, effective use of the IFTA requires the exploitation of the design freedoms so that the algorithm can modify the complex transmission values of the DOE, while maintaining the desired performance objective in the image plane [6].

By contrast, the philosophy behind unidirectional algorithms is that, if the DOE can be characterized by a finite set of quantized parameters (e.g., phase levels), a finite (albeit large) number of permutations of these parameters exists. The objective of the algorithm is to find the permutation that achieves the optimization in an efficient manner. Two examples of unidirectional algorithms are gradient descent methods and annealing algorithms [15–17]. In these algorithms, the present DOE is a function of the previous DOE and the performance generated by it. When the model of the optical system cannot be inverted, unidirectional algorithms must be used.

The results of the direct solution of problem 1, using both the IFTA and simulated annealing, are represented in figure 9 and summarized in table 3. Although there is a notable improvement in performance over quantization, it is again impossible to make general statements about the effectiveness of simulated annealing over IFTA from this example. The diffraction efficiency of the IFTA-designed array generator is lower than that of the annealed array generator, but their performances are otherwise comparable. It is true, however, that simulated annealing requires more computing time than the IFTA.

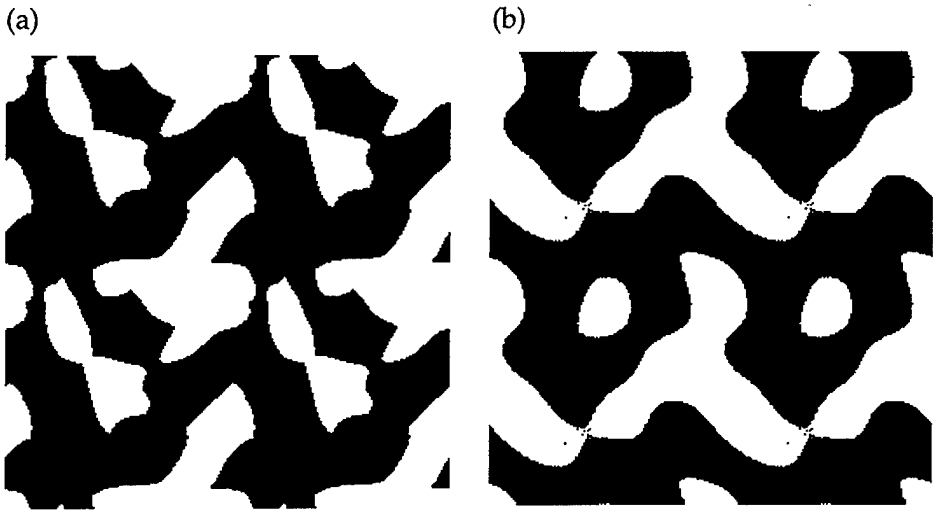

Figure 9. Representation of direct design of nonseparable array generators: (a) IFTA design; (b) annealed design (two replications of the unit cells are shown).

3.2 Example 2: 8-Phase-Level 7 × 7 Array Generator

The second design example is for an 8-phase-level 7 × 7 array generator that has the nonuniform intensity distribution $|q(x,y)|^2$ indicated below.

$\|q(x,y)\|^2$	$x=-3$	$x=-2$	$x=-1$	$x=0$	$x=1$	$x=2$	$x=3$
$y=-3$	0.0003	0.0019	0.0051	0.0068	0.0051	0.0019	0.0003
$y=-2$	0.0019	0.0103	0.0248	0.0328	0.0248	0.0103	0.0019
$y=-1$	0.0051	0.0248	0.0583	0.0766	0.0583	0.0248	0.0051
$y=0$	0.0068	0.0328	0.0766	0.0000	0.0766	0.0328	0.0068
$y=1$	0.0051	0.0248	0.0583	0.0766	0.0583	0.0248	0.0051
$y=2$	0.0019	0.0103	0.0248	0.0328	0.0248	0.0103	0.0019
$y=3$	0.0003	0.0019	0.0051	0.0068	0.0051	0.0019	0.0003

Unlike the 5 × 5 fanout, the spot spacing along the horizontal and vertical axes is unequal: $d_x \times d_y = 160 \times 80$ μm^2. The wavelength λ = 850 nm and the focal length f = 50 mm; therefore, the grating period $W_x \times W_y$ = 265.625 × 531.25 μm^2. The size of the DOE was fixed at 1 × 1 cm^2, and so, for ease of fabrication and design, I selected the minimum feature $\Delta_x \times \Delta_y = 2.1 \times 4.2$ μm^2.

I designed a nonseparable DOE using a direct approach that I implemented using the IFTA. I selected the number of features in a unit cell to be 128 × 128, which yields a grating period of 268.8 × 537.6 μm^2. The unit period was replicated 37 × 18 times to produce an element 9.9456 × 9.6768 mm^2. Given these parameters, the spot spacing is 158.11 × 79.06 μm^2. (Note that a separable design is not possible because the DOE has eight phase levels—when crossed, an 8-level, one-dimensional DOE does not yield an 8-level, two-dimensional DOE.)

A diffraction efficiency upper bound of 91.15 percent is generated by the phase $\theta_{ub}(x, y)$.

$\theta_{ub}(x,y)$	$x=-3$	$x=-2$	$x=-1$	$x=0$	$x=1$	$x=2$	$x=3$
$y=-3$	1.2566	0.2038	−0.1017	−2.9513	−0.1017	0.2038	1.2566
$y=-2$	1.1104	0.5581	−0.7317	−2.7790	−0.7317	0.5581	1.1104
$y=-1$	0.6649	−0.2590	−1.8587	2.5672	−1.8587	−0.2590	0.6649
$y=0$	−2.9513	−2.7790	2.5672	0.0000	2.5672	−2.7790	−2.9513
$y=1$	0.6649	−0.2590	−1.8587	2.5672	−1.8587	−0.2590	0.6649
$y=2$	1.1104	0.5581	−0.7317	−2.7790	−0.7317	0.5581	1.1104
$y=3$	1.2566	0.2038	−0.1017	−2.9513	−0.1017	0.2038	1.2566

The phase assumes an 8-level phase-only DOE; however, no symmetry constraints were imposed on the problem—the symmetry exhibited in the phase results from the symmetry in the array intensity. The magnitude and phase of the upper bound $Q_{ub}(u, v)$ in the spatial frequency domain are represented in figures 10(a) and (b). An alternate representation is the complex plane representation in figure 11. The IFTA must take these data points and map them to eight equally spaced discrete values on the unit circle.

The phase of the element designed by the IFTA is represented in figure 12. The intensity $|p(x, y)|^2$ generated by this element follows.

$\lvert p(x,y)\rvert^2$	$x=-3$	$x=-2$	$x=-1$	$x=0$	$x=1$	$x=2$	$x=3$
$y=-3$	0.0003	0.0016	0.0046	0.0062	0.0046	0.0016	0.0003
$y=-2$	0.0016	0.0093	0.0235	0.0307	0.0235	0.0093	0.0016
$y=-1$	0.0046	0.0234	0.0541	0.0698	0.0541	0.0234	0.0046
$y=0$	0.0062	0.0305	0.0699	0.0000	0.0699	0.0305	0.0062
$y=1$	0.0046	0.0234	0.0541	0.0698	0.0541	0.0234	0.0046
$y=2$	0.0016	0.0093	0.0235	0.0307	0.0235	0.0093	0.0016
$y=3$	0.0003	0.0016	0.0046	0.0062	0.0046	0.0016	0.0003

The diffraction efficiency of the generated array is 91.97 percent, which is greater than the upper bound due to the presence of error: $e_{\text{int}} = 6.90 \times 10^{-6}$ for $\alpha_{\text{min}} = 0.92$. The noise fluctuations per spot $e_{\text{rms}} = 0.376 \times 10^{-3}$. Therefore, the DOE satisfies the design specifications exceptionally well.

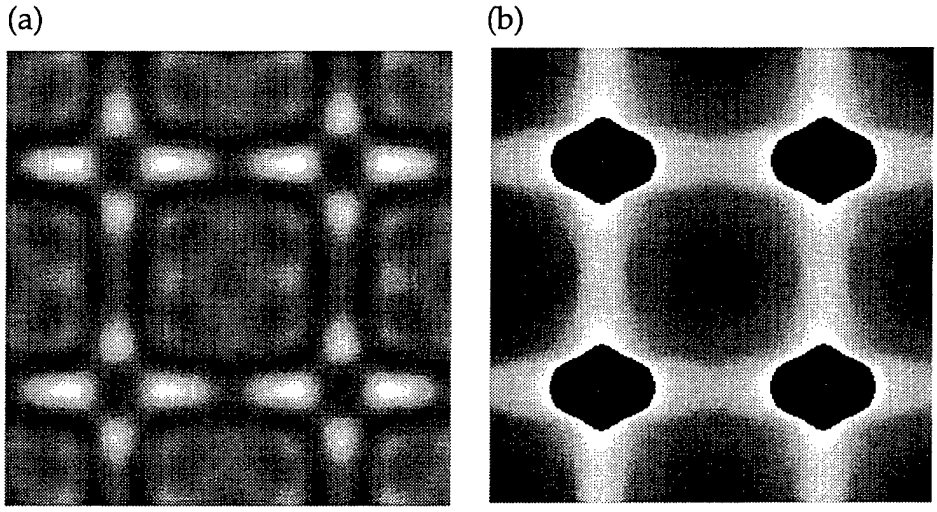

Figure 10. Representation of $Q_{ub}(u,v)$ for a 7×7 fanout (two periods in the spatial frequency domain (u,v) are shown in (a) $|Q_{ub}(u,v)|$, and (b) arg $\{Q_{ub}(u,v)\}$).

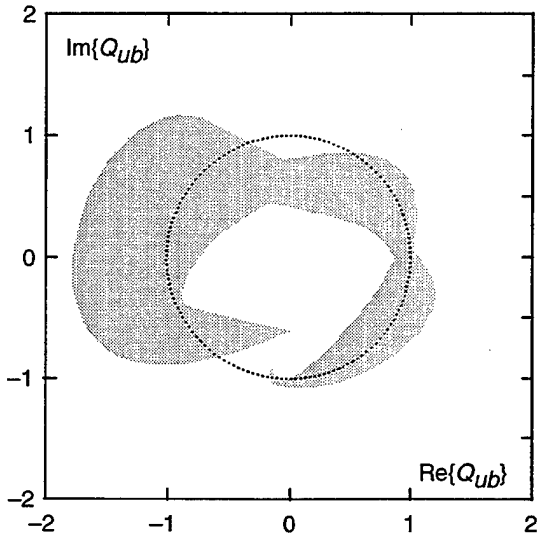

Figure 11. Complex plane representation of $Q_{ub}(u,v)$.

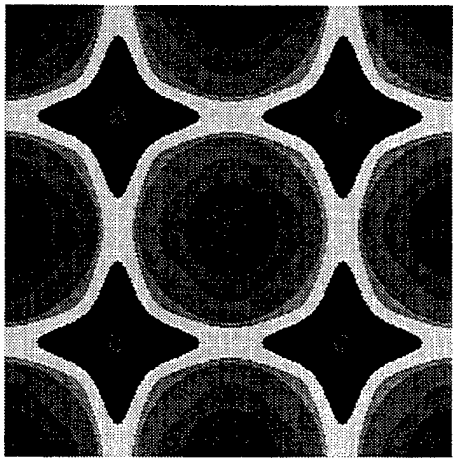

Figure 12. Phase representation of 8-level phase-only array generator (two replications of the unit cell are shown).

Fabrication of the 8-level element requires the three binary masks shown in figure 13. White indicates the areas to be etched; black indicates the areas in which etching should not take place. The horizontal scale of the masks is half that of the phase function, due to the different horizontal and vertical spacings between spots. The mask set was used by Honeywell to fabricate the element, which is currently being characterized at the Army Research Laboratory.

4. Summary

In this work, I used two applications of DOEs in an optical A/D converter to highlight the procedure for designing diffractive elements using scalar diffraction theory. The selection of models for the optical system and fabrication technology, as well as the proper statement of the design in terms of optimization, is essential to this procedure. I designed high-efficiency, low-noise elements using phase, amplitude, and scale design freedoms.

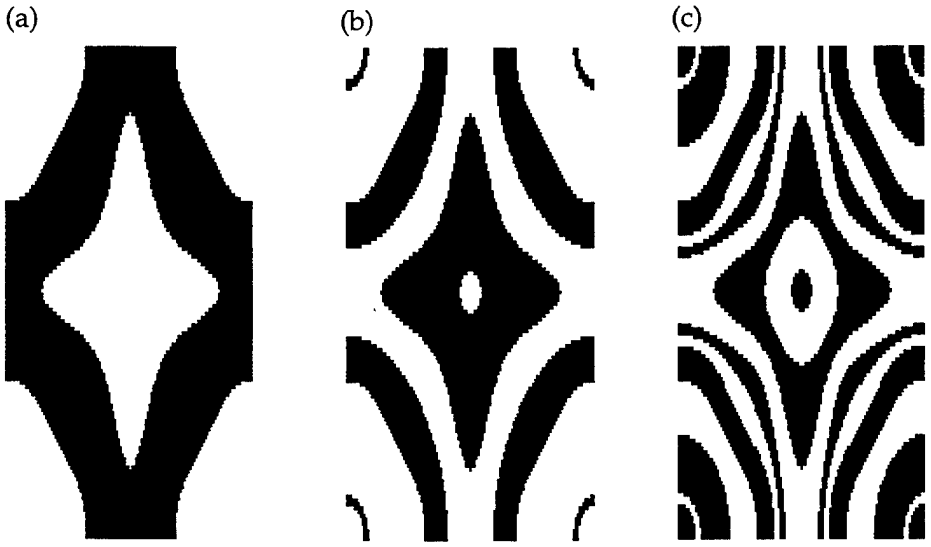

Figure 13. Binary amplitude mask set necessary to fabricate an 8-level phase-only array generator (single period representation of mask used to etch (a) π-phase, (b) $\pi/2$-phase, and (c) $\pi/4$-phase).

References

1. J. N. Mait, *Design of binary- and multi-phase Fourier gratings for array generation*, J. Opt. Soc. Am. **A 7**, 1514–1528 (1990).

2. J. N. Mait, *Understanding diffractive optical design in the scalar domain*, J. Opt. Soc. Am. **A 12**, 2145–2158 (1995).

3. B. L. Shoop and J. W. Goodman, *A first-order error diffusion modulator for optical over sampled A/D conversion*, Opt. Commun. **37**, 167–172 (1993).

4. J. W. Goodman, *Introduction to Fourier Optics*, McGraw-Hill, New York, Ch. 3 (1968).

5. M. Stern, *Binary Optics Fabrication*, Micro-optics: Elements, systems, and applications, H.-P. Herzig, ed. (Taylor and Francis Ltd, London, to be printed in 1997).

6. F. Wyrowski, *Digital holography as part of diffractive optics*, Rep. Prog. Phys. **54**, 1481–1571 (1991).

7. F. Wyrowski, *Upper bound of the diffraction efficiency of diffractive phase elements*, Opt. Lett. **16**, 1915–1917 (1991).

8. U. Krackhardt, J. N. Mait, and N. Streibl, *Upper bound on the diffraction efficiency of phase-only fan-out elements*, Appl. Opt. **31**, 27–37 (1992).

9. H. Dammann and K. Görtler, *High-efficiency in-line multiple imaging by means of multiple phase holograms*, Opt. Commun. **3**, 312–315 (1971).

10. R. L. Morrison, *Symmetries that simplify design of spot array phase gratings*, J. Opt. Soc. Am. A **9**, 464–471 (1992).

11. J. N. Mait, *Fourier Array Generators*, in Micro-optics: Elements, systems, and applications, H.-P. Herzig, ed. (Taylor and Francis Ltd, London, to be printed in 1997).

12. C. Zhou and L. Liu, *Numerical study of Dammann array illuminators*, Appl. Opt. **34**, 5961–5969 (1995).

13. J. R. Fienup, *Iterative method applied to image reconstruction and to computer-generated holograms*, Opt. Eng. **19**, 297–306 (1980).

14. N. C. Gallagher and B. Liu, *Method for computing kinoforms that reduces image reconstruction error*, Appl. Opt. **12**, 2328–2335 (1973).

15. B. K. Jennison, J. P. Allebach, and D. W. Sweeney, *Iterative approaches to computer-generated holography*, Opt. Eng. **28**, 629–637 (1989).

16. J. Turunen, A. Vasara, and J. Westerholm, *Kinoform phase relief synthesis: a stochastic method*, Opt. Eng. **28**, 1162–1167 (1989).

17. M. R. Feldman and C. C. Guest, *High efficiency hologram encoding for generation of spot arrays*, Opt. Lett. **14**, 479–481 (1989).

Appendix A

The following tables indicate the intensity responses of the array generators designed in section 3.

Upper Bound:

$\lvert p(x,y)\rvert^2$	$x=-2$	$x=-1$	$x=0$	$x=1$	$x=2$
$y=-2$	0.0315	0.0315	0.0315	0.0315	0.0315
$y=-1$	0.0315	0.0315	0.0315	0.0315	0.0315
$y=0$	0.0315	0.0315	0.0315	0.0315	0.0315
$y=1$	0.0315	0.0315	0.0315	0.0315	0.0315
$y=2$	0.0315	0.0315	0.0315	0.0315	0.0315

Dammann Grating:

$\lvert p(x,y)\rvert^2$	$x=-2$	$x=-1$	$x=0$	$x=1$	$x=2$
$y=-2$	0.0240	0.0239	0.0240	0.0239	0.0240
$y=-1$	0.0239	0.0239	0.0239	0.0239	0.0239
$y=0$	0.0240	0.0239	0.0240	0.0239	0.0240
$y=1$	0.0239	0.0239	0.0239	0.0239	0.0239
$y=2$	0.0240	0.0239	0.0240	0.0239	0.0240

Quantized Upper Bound:

$\lvert p(x,y)\rvert^2$	$x=-2$	$x=-1$	$x=0$	$x=1$	$x=2$
$y=-2$	0.0225	0.0265	0.0239	0.0365	0.0294
$y=-1$	0.0244	0.0347	0.0333	0.0532	0.0454
$y=0$	0.0187	0.0395	0.0298	0.0395	0.0187
$y=1$	0.0454	0.0532	0.0333	0.0347	0.0244
$y=2$	0.0294	0.0365	0.0239	0.0265	0.0225

IFTA Design:

$\lvert p(x,y)\rvert^2$	$x=-2$	$x=-1$	$x=0$	$x=1$	$x=2$
$y=-2$	0.0284	0.0254	0.0295	0.0306	0.0266
$y=-1$	0.0272	0.0298	0.0278	0.0262	0.0276
$y=0$	0.0254	0.0296	0.0289	0.0296	0.0254
$y=1$	0.0276	0.0262	0.0278	0.0298	0.0272
$y=2$	0.0266	0.0306	0.0295	0.0254	0.0284

Annealed Design:

$\lvert p(x,y)\rvert^2$	$x=-2$	$x=-1$	$x=0$	$x=1$	$x=2$
$y=-2$	0.0316	0.0315	0.0331	0.0285	0.0285
$y=-1$	0.0302	0.0318	0.0297	0.0297	0.0313
$y=0$	0.0301	0.0296	0.0322	0.0296	0.0301
$y=1$	0.0313	0.0297	0.0297	0.0318	0.0302
$y=2$	0.0285	0.0285	0.0331	0.0315	0.0316

Distribution

Admnstr
Defns Techl Info Ctr
Attn DTIC-OCP
8725 John J Kingman Rd Ste 0944
FT Belvoir VA 22060-6218

Hdqtrs Dept of the Army
Attn DAMO-FDQ MAJ M McGonagle
400 Army Pentagon
Washington DC 20310-0460

United States Military Academy
Attn Cadet W Johnson
PO Box 1654
West Point NY 10997

United States Military Academy
Photonics Rsrch Ctr
Attn MAJ B Shoop
West Point NY 10996

George Mason Univ
Elect & Computer Engrg Dept
Attn Prof R Athale
Fairfax VA 22030

Georgia Inst of Technl
School of Physics
Attn Prof D O'Shea
Atlanta Georgia 30332

US Army Rsrch Lab
Attn AMSRL-PS-ED L Poli
FT Monmouth NJ 07703-5601

Army Rsrch Lab
Attn AMSRL-SE-EM G Simonis
Attn AMSRL-CI-LL Tech Lib (3 copies)
Attn AMSRL-CS-AL-TA Mail & Records Mgmt
Attn AMSRL-CS-AL-TP Techl Pub (3 copies)
Attn AMSRL-SE-E J Pellegrino
Attn AMSRL-SE-SR A Filipov
Attn AMSRL-SE-EE B Lawler
Attn AMSRL-SE-EO D Mackie
Attn AMSRL-SE-EO D Prather
Attn AMSRL-SE-EO D Smith
Attn AMSRL-SE-EO G Euliss
Attn AMSRL-SE-EO J Goff
Attn AMSRL-SE-EO J Mait
Attn AMSRL-SE-EO J van der Gracht
Attn AMSRL-SE-EO L Harrison
Attn AMSRL-SE-EO N Gupta
Attn AMSRL-SE-EO S Sarama
Attn AMSRL-SE-EO T Tayag
Adelphi MD 20783-1197

REPORT DOCUMENTATION PAGE

Form Approved
OMB No. 0704-0188

1. AGENCY USE ONLY *(Leave blank)*	2. REPORT DATE	3. REPORT TYPE AND DATES COVERED
	February 1997	Final, from August 1995–July 1996

4. TITLE AND SUBTITLE
Diffractive Design: Two Examples from an Optical Analog-to-Digital Converter

5. FUNDING NUMBERS
DA PR: 61102
PE: 61102.AH44

6. AUTHOR(S)
Joseph N. Mait

7. PERFORMING ORGANIZATION NAME(S) AND ADDRESS(ES)
U.S. Army Research Laboratory
Attn: AMSRL-SE-EO
2800 Powder Mill Road
Adelphi, MD 20783-1197

8. PERFORMING ORGANIZATION REPORT NUMBER
ARL-MR-336

9. SPONSORING/MONITORING AGENCY NAME(S) AND ADDRESS(ES)
U.S. Army Research Laboratory
2800 Powder Mill Road
Adelphi, MD 20783-1197

10. SPONSORING/MONITORING AGENCY REPORT NUMBER

11. SUPPLEMENTARY NOTES
AMS code: 611102.H44
ARL PR No: 5AE152

12a. DISTRIBUTION/AVAILABILITY STATEMENT
Approved for public release; distribution unlimited.

12b. DISTRIBUTION CODE

13. ABSTRACT *(Maximum 200 words)*

In this report, I present the designs of two diffractive optical array generators used in an optical analog-to-digital converter. The designs follow a procedure that I developed for the design of general diffractive optical elements. I consider both separable and nonseparable approaches to designing a 5×5 binary-phase fanout, and discuss indirect and direct optimizations for the nonseparable approach. I use a nonseparable approach with direct optimization to design an 8-phase-level 7×7 array generator.

14. SUBJECT TERMS
Diffractive optics, optical A/D

15. NUMBER OF PAGES
28

16. PRICE CODE

17. SECURITY CLASSIFICATION OF REPORT	18. SECURITY CLASSIFICATION OF THIS PAGE	19. SECURITY CLASSIFICATION OF ABSTRACT	20. LIMITATION OF ABSTRACT
Unclassified	Unclassified	Unclassified	UL

NSN 7540-01-280-5500

Standard Form 298 (Rev. 2-89)
Prescribed by ANSI Std. Z39-18
298-102